Photoluminescence properties of red-emitting Mn2+-activated CaAlSiN3 phosphor for white-LEDs

ECS Journal of Solid State Science and Technology, **2** (4) R70-R75 (2013)
2162-8769/2013/2(4)/R70/6/$31.00 © The Electrochemical Society

Photoluminescence Properties of Red-Emitting Mn^{2+}-Activated $CaAlSiN_3$ Phosphor for White-LEDs

Zhijun Zhang,[a,b] Anneke C. A. Delsing,[a] Peter H. L. Notten,[a,*] Jingtai Zhao,[b] Pieter Dorenbos,[c] and Hubertus T. Hintzen[a,z]

[a]*Energy Materials and Devices, Department of Chemical Engineering and Chemistry, Eindhoven University of Technology, 5600 MB Eindhoven, The Netherlands*
[b]*Key Laboratory of Transparent Opto-Functional Inorganic Materials of Chinese Academy of Sciences, Shanghai Institute of Ceramics, Shanghai 200050, China*
[c]*Luminescent Materials Research Group, Delft University of Technology, 2629 JB Delft, The Netherlands*

Mn^{2+}-doped $CaAlSiN_3$ phosphors have been prepared by a solid-state reaction method at high temperature and the solubility of Mn^{2+} in the host lattice as well as their photoluminescence properties were investigated. In $CaAlSiN_3$, not only Ca^{2+} sites, but also Al^{3+} sites can be substituted by Mn^{2+} ions. $CaAlSiN_3 : Mn^{2+}$ absorbs blue light in the spectral range of 440–460 nm, and exhibits a broad band emission in the wavelength range of 475–750 nm, which can be ascribed to the $^4T_1$ (^4G) $\rightarrow$ $^6A_1$ (^6S) transition of Mn^{2+} located at two different sites in $CaAlSiN_3$. The emission bands at lower energy (15,950 cm^{-1} or 627 nm) and higher energy (18,250 cm^{-1} or 548 nm) are assigned to the Mn^{2+} locating at the Al site (Mn_{Al}) and Ca site (Mn_{Ca}), respectively with energy transfer from Mn_{Ca} to Mn_{Al}. In addition, the integral luminescence intensity only decreases to about 94% at 150°C of the value at 50°C, which is of great interest for the applications of white-LEDs.
 [DOI: 10.1149/2.017304jss]

Manuscript submitted October 29, 2012; revised manuscript received January 28, 2013. Published February 8, 2013.

Multinary nitrides and oxynitrides have attracted more attentions in recent years. They have been extensively investigated as host lattices for phosphors when activated by rare-earth ions, such as M^ISiN_2: Eu^{2+}, Ce^{3+} (M^I = Ca, Sr, Ba),[1,2] $M^I_2Si_5N_8 : Eu^{2+}$, Ce^{3+} [M^I = Ca, Sr, Ba],[3–8] $M^{II}AlSiN_3 : Eu^{2+}$, Ce^{3+} (M^{II} = Ca, Sr),[9–12] α-SiAlON : RE (RE = Eu^{2+}, Ce^{3+}, Yb^{2+}, Tb^{3+}, Pr^{3+}, Sm^{3+}),[13–16] $M^ISi_2O_{2-\delta}N_{2+2/3\delta}$: Eu^{2+}, Ce^{3+} (M^I = Ca, Sr, Ba),[17,18] $M^ISi_xAl_{2-x}O_{4-x}N_x : Eu^{2+}$ (M^I = Ca, Sr, Ba),[19] $M^{III}{}_ySi_{6-z}Al_{z-y}O_{z+y}N_{8-z-y}$ (M^{III} = 2Li, Mg, Ca, Sr, Ba).[20] These nitrides and oxynitrides have many advantages including strong absorption from UV to blue, high quantum efficiency, chemical stability as well as excellent thermal characteristics, allowing them to be widely used as efficient conversion phosphors for white-LEDs.

Rare-earth ions with 4*f* - 5*d* transitions (e. g. Eu^{2+}, Ce^{3+}) show long wavelength absorption and emission in nitride, due to the high covalency and large crystal splitting effect of nitrogen anion.[21] The nitrides and oxynitrides activated by these rare-earth ions have been demonstrated to be promising efficient conversion phosphors for white-LEDs.[22] More recently, interests also have been focused on the luminescence properties of transition metals, such as Mn^{2+}.[23–25] The wavelength position of the emission band of Mn^{2+}, as a typical transition ion, also depends strongly on the host lattice, including the strength of the ligand field and the coordination number (CN). In general, Mn^{2+} usually gives a green emission when it is located on a lattice with weak crystal-field, whereas it shows an orange to deep red emission on a strong crystal-field site. On the other hand, the coordination number also has a great effect on the emission color: the Mn^{2+} ions emit green light when it is tetrahedrally coordinated (CN = 4) in the lattice whereas it emits red light in octahedral coordination (CN = 6).[26] Mn^{2+}-doped inorganic phosphors have been used as phosphors for white-LEDs, e.g. $Ba_2ZnS_3 : Mn^{2+}$ (Red),[23,27] fluorescent lamps, such as $BaAl_{12}O_{19} : Mn^{2+}$ (Green)[28] and Zn_2SiO_4: Mn^{2+} (Green),[29] and cathode-ray tubes (CRT), e.g. $ZnS : Mn^{2+}$ (Orange),[30,31] $Zn_3(PO_4)_2 : Mn^{2+}$ (Red).[24,25] There are few reports with regard to the luminescence properties of Mn^{2+} in nitride host lattices except some publications on $M^{IV}SiN_2 : Mn^{2+}$ (M^{IV} = Mg, Zn, Ca),[32,33] $M^I_2Si_5N_8 : Mn^{2+}$ (M^I = Ca, Sr, Ba),[34] $MgSiN_2 : Mn^{2+}$,[35] $ZnGeN_2 : Mn^{2+}$,[36] γ-AlON : Mn^{2+}, Mg^{2+}.[37] However, Mn^{2+} doped $M_2Si_5N_8$ and $MgSiN_2$ show weak absorption in the range of 350–470 nm due to the forbidden *d* - *d* transitions of Mn^{2+}. As for the white-LEDs applications this absorption has to be increased by use of suitable sensitizer ions, such as Ce^{3+}, $Mn^{2+} : MgSiN_2$.[38]

Recently, a new quaternary nitride system, $CaAlSiN_3$ has drawn much attention for its applications in the white-LEDs when doped with Eu^{2+} or Ce^{3+}.[10,39] $CaAlSiN_3$ is isostructural with ASi_2N_3 (A = Li, Na) and crystallizes in $Cmc2_1$ space group.[9] The Ca atom is located at the channels built up by the six-membered rings of $(Al/Si)N_4$ tetrahedra and directly coordinated with five nitrogen atoms cross over the unit cell (Figure 1). The Al and Si atoms are randomly distributed on the same tetrahedral sites and connected with nitrogen atoms to form the vertex-linked $M^V{}_6N_{18}$ (M^V = Al, Si) rings.[40] $CaAlSiN_3 : Eu^{2+}$ and $CaAlSiN_3 : Ce^{3+}$ exhibit efficient red and yellow-orange emission respectively under blue irradiation.[10,39] In the present work, we focus on investigating the luminescence properties of Mn^{2+} in $CaAlSiN_3$ and explore its potential possibilities to be used as a new kind of LED conversion phosphor, which is up to now only claimed but not proofed.[41]

Experimental

Starting Materials.— Ca_3N_2 (Alfa, 98%, powder), AlN (Tokuyama Chemical Co., Ltd., F-grade), α-Si_3N_4 (Permascand, P95H, α content, 93.2%, oxygen content: ∼1.5%) and Mn powder (Alfa, > 99%) are used as the as-received raw materials.

Syntheses of Mn^{2+}-doped $CaAlSiN_3$.— $CaAlSiN_3 : Mn^{2+}$ powder samples were prepared by a solid-state reaction method at high temperature. Appropriate amounts of starting materials were firstly weighed out, thoroughly mixed and ground in an agate mortar. The powder mixtures were fired in molybdenum crucibles at 1600 °C for 2 h in a horizontal tube furnace under N_2-H_2 (10%) atmosphere. After firing, the samples were gradually cooled down in the furnace. Subsequently, the resulting powder was reground and pressed into pellets of 1 cm in diameter under 170 MPa, then fired at 1750 °C for 2 h in a molybdenum crucible under flowing N_2-H_2 (10%) atmosphere. After sintering, these samples were gradually cooled down to room temperature in the furnace. There was no apparent reaction of the prepared samples with the Mo crucibles. All processes were handled in a dry glove box flushed with dry nitrogen because of air and water sensitivity of some starting materials.

X-ray diffraction data collection and analysis.— All measurements were performed on finely ground samples, which were analyzed by X-ray powder diffraction (XRD) (Bruker, D4 Endeavor X-ray Diffractometer) using Cu K_α radiation at 40 kV and 40 mA with a graphite monochromator. The 2θ ranges of all the data sets are from 10 to 80° using step scan with a step size of 0.02° in 2θ

*Electrochemical Society Active Member.
zE-mail: h.t.hintzen@tue.nl

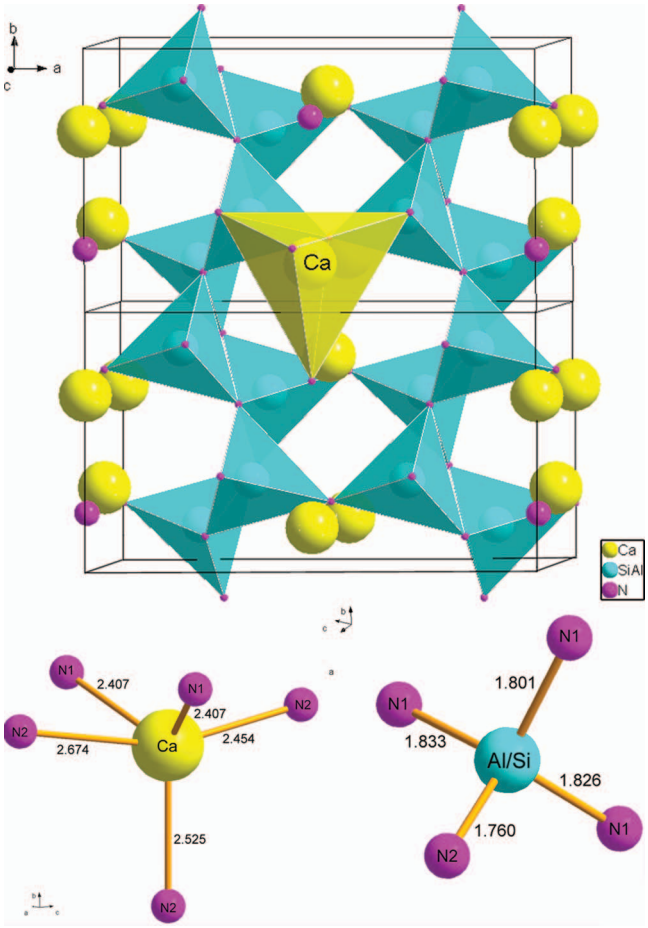

Figure 1. Crystal structure of $CaAlSiN_3$, and the coordination environment of Ca, Al/Si atoms, as well as Ca-N, Al/Si-N distances (Å) in $CaAlSiN_3$.

and a count time of 1 s. The XRD measurements were performed at room temperature in air. The cell parameters of $CaAlSiN_3$: Mn^{2+} were determined from the X-ray powder diffraction patterns using the indexing program Fullprof.[42]

X-ray absorption near-edge structure (XANES).— Mn K-edge of X-ray absorption near-edge structure (XANES) spectra at about 6540 eV were recorded at room temperature at Shanghai Synchrotron Radiation Facility (SSRF, China) in transmission modes. The X-ray light source was from the BL14W1 beam line at the SSRF. The electron energy in the storage ring was 3.5 GeV, with a current of 200 mA and the emission angle of the light was 1.5 × 0.1 $mrad^2$. The beam size can be focused to 0.3 mm × 0.3 mm. The scanning range was from 6500 to 6650 eV. The energy steps were 0.2 eV (from 6500 to 6650 eV), which was appropriate for obtaining a clear Mn K-edge XANES spectrum. The information on the valence state and local structure of the element of interest can be obtained from the XANES spectra based on the energy, shape and fine structure of the edges.

Optical measurements.— The diffuse reflectance, emission and excitation spectra of the samples were measured at room temperature by a Perkin Elmer LS 50B spectrophotometer equipped with a Xe flash lamp. The reflection spectra were calibrated with the reflection of black felt (reflection 3%) and white barium sulfate ($BaSO_4$, reflection ~ 100%) in the wavelength region of 230–700nm. The excitation and emission slits were set at 15 nm. The emission spectra were corrected by dividing the measured emission intensity by the ratio of the observed spectrum of a calibrated W-lamp and its known spectrum from 300 to 900 nm. Excitation spectra were automatically

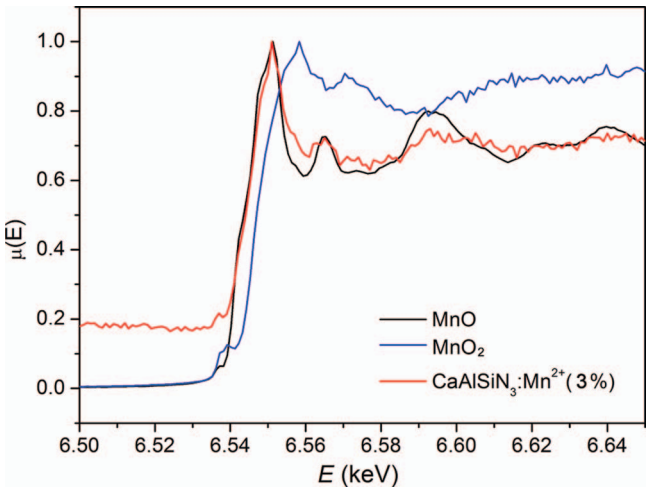

Figure 2. The X-ray absorption near-edge structure (XANES) spectra of Mn^{2+} in $CaAlSiN_3$, and the standard samples MnO and MnO_2.

corrected for the variation in the lamp intensity (and thus for the spectral dependence of the excitation energy) by a second photomultiplier and a beam-splitter. All luminescence spectra were measured with a scan speed of 400 nm/min at room temperature in air. The temperature dependent emission measurement was carried out by the special equipment made by University of Jena under excitation with 450 nm from room temperature to 200°C with a heating rate of 8°C/min, and the temperature was hold for 5 min before starting the measurement.

Results and Discussion

Valency State of Mn in $CaAlSiN_3$.— It can be observed from Figure 2 that the position of the K-edge of Mn in $CaAlSiN_3$ is similar to that of MnO (6540.6 eV), locating at lower energy than that of MnO_2 (6541.6 eV), which means that Mn in $CaAlSiN_3$ is found in the divalent state. However, the signal of the extended X-ray absorption fine structural (EXAFS) data is too weak to get information about the number of Mn^{2+} sites and about the local structure of Mn^{2+} in $CaAlSiN_3$.

Phase formation and the solubility of Mn^{2+} in $CaAlSiN_3$.— According to the powder XRD patterns (Figure 3), the Mn-doped $CaAlSiN_3$ samples were obtained as nearly single phase material with $CaAlSiN_3$ structure (ICSD no: 161796). Like in the case of $CaAlSiN_3$:

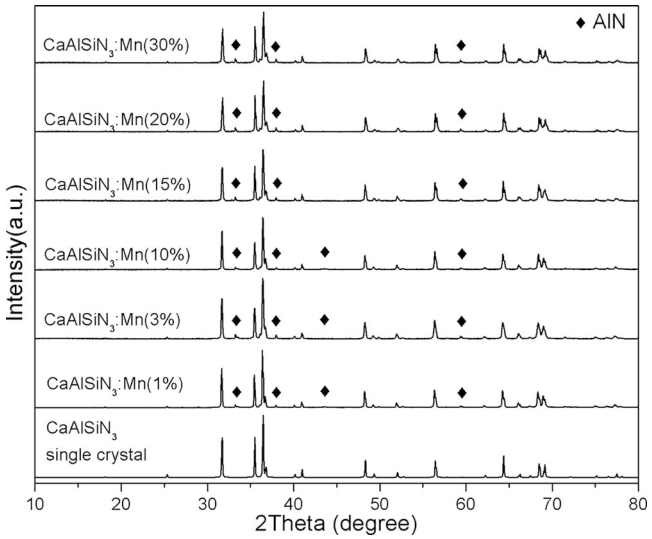

Figure 3. Powder X-ray diffraction patterns of Mn-doped $CaAlSiN_3$.

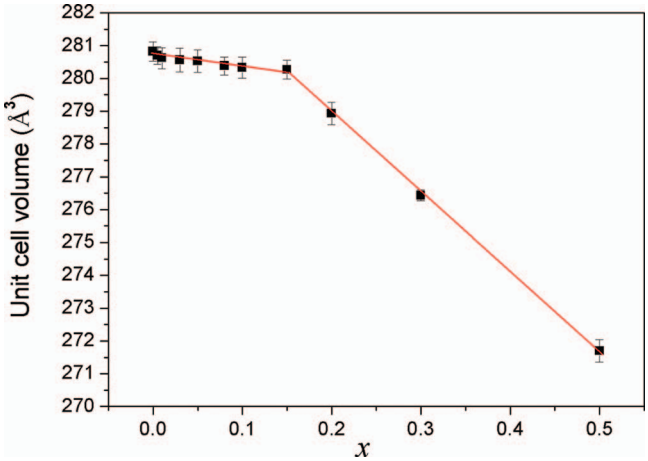

Figure 4. The relationship between unit cell volume of $Ca_{1-x}Mn_xAlSiN_3$ and the x value. The value for $MnAlSiN_3$ (i.e. $x = 1$, JCPDS : 50-0749) is taken from Ref. 44.

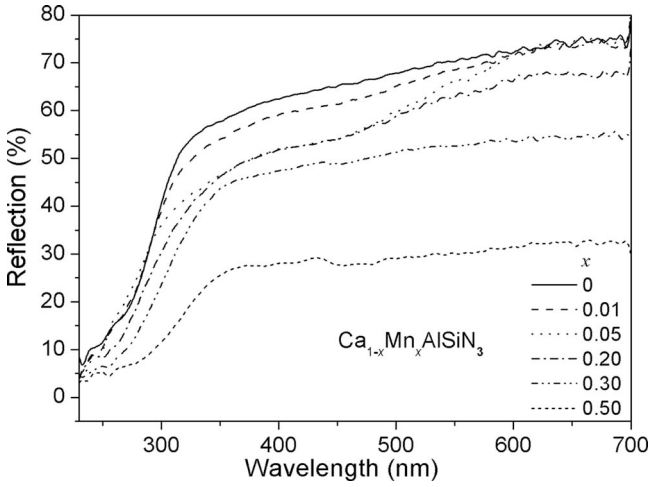

Figure 5. The diffuse reflection spectra of $Ca_{1-x}Mn_xAlSiN_3$ ($0 \le x \le 0.5$) samples.

Ce^{3+}, Li^+,[10] it is difficult to obtain undoped and Mn-doped $CaAlSiN_3$ samples as a single phase material according to the stoichiometric composition. It was found that Al/Si disorderly occupies the 8*b* site in the space group of $Cmc2_1$ with a ratio of about 1/2 with a more appropriate formula $CaAl_{1-4\delta/3}Si_{1+\delta}N_3$ ($\delta = 0.3$ - 0.4) instead of 1/1 proposed for an ideal $CaAlSiN_3$, probably due to the incomplete reaction resulting in a significantly lower Al solubility in $CaAlSiN_3$.[10] Thus, a small amount of AlN can be detected for undoped and Mn-doped $CaAlSiN_3$ samples.

The unit cell volume of $Ca_{1-x}Mn_xAlSiN_3$ decreases with increasing Mn^{2+} concentration (Figure 4), as expected for Mn^{2+} ($r = 0.75$ Å, CN = 5, $r = 0.83$ Å, CN = 6) being smaller than Ca^{2+} ($r = 1.00$ Å, CN = 6).[43] In agreement with Ca^{2+} by Mn^{2+} replacement, the unit cell volume of $Ca_{1-x}Mn_xAlSiN_3$ extrapolated for high Mn^{2+} to $x = 1$ concentration agrees with that of $MnAlSiN_3$ (JCPDS : 50-0749, the cell volume of $MnAlSiN_3$, i.e. $x = 1.0$, was calculated from D. P. Thompson[44]). However, as a function of the Mn^{2+} concentration, two linear regimes can be discriminated: for high Mn^{2+} concentrations ($x > 0.15$) the dependence is stronger than for low Mn^{2+} concentrations ($x < 0.15$), with a bending point at about 15 at% Mn^{2+} ($x = 0.15$). The weaker dependence can be explained by assuming that at low Mn concentrations, Mn^{2+} not only occupies the Ca^{2+} position, but in addition also partly occupies the Al^{3+} site with Mn^{2+} ($r = 0.66$ Å, CN = 4) larger than Al^{3+} ($r = 0.39$ Å, CN = 4). The Al^{3+} by Mn^{2+} replacement can be charge compensated by Al^{3+}/Si^{4+} replacement or N^{3-}/O^{2-} replacement. Unfortunately, a Rietveld refinement of the XRD patterns with Mn^{2+} substituted on both the Ca^{2+} as well as Al^{3+} sites or XANES/EXAFS measurements did not allow us to confirm this interpretation, which however is fully supported by luminescence measurements, as discussed in the next section.

Diffuse reflection spectra.— Figure 5 shows the diffuse reflection spectra of undoped and Mn^{2+}-doped $CaAlSiN_3$ samples. For undoped $CaAlSiN_3$ show a drastic drop in reflection in the ultraviolet (UV) range around 300 nm with an estimated bandgap at about 240 nm (5.2 eV), essentially corresponding to the valence-to-conduction band transitions of $CaAlSiN_3$ host lattice. The value of the bandgap is close to the results published.[10,39] The intense reflection in the visible spectral range is in agreement with the observed gray-white daylight color of undoped $CaAlSiN_3$. For Mn^{2+}-doped $CaAlSiN_3$, there are several weak absorption bands can be observed in the wavelength range of 350–600 nm, which can be attributed to the transitions from the $^6A_1$ (^6S) ground state of Mn^{2+} to its excited states. In contrast to the undoped sample, the daylight color of Mn^{2+}-doped $CaAlSiN_3$ shows gray-white to light red color, varying with Mn^{2+} concentration as a result of the absorption by Mn^{2+} ion the visible range of 350–600 nm. Additionally, the absorption edge of $CaAlSiN_3 : Mn^{2+}$ shifts to longer wavelength, corresponding to the decrease in the optical bandgap with increasing Mn^{2+} concentration. According to the band and electronic structure calculation results, the bottom of the conduction band (CB) of $CaAlSiN_3$ is mainly composed of Ca 3*d* orbitals, and Al/Si 3*s*/3*p* orbitals are hybridized at higher energy, while the top of valence band (VB) are dominated by the 2*p* states of N atoms.[45] Thus, the VB → CB inter-band transition of $CaAlSiN_3$ is corresponding to a transition from N 2*p* to Ca 3*d* and Al/Si 3*s*/3*p* energy levels. The red-shift of the optical bandgap of $CaAlSiN_3 : Mn^{2+}$ with increasing Mn^{2+} concentration can be ascribed to the spin-exchange interaction between the Mn^{2+} ions and the band electrons (the so-called *s* - *d* and *p* - *d* interactions), which gives rise to a negative and a positive correction to the energy of the conduction and valence bands, respectively, and leads to a redshift of the optical bandgap.[46]

Photoluminescence properties of Mn^{2+} in $CaAlSiN_3$.— In general, it is well known that the $3d^5$ multiplet energies of Mn^{2+} in the host lattice strongly depends on the crystal field and the covalent interaction with the host lattice because the 3*d* electrons of the transition metal Mn^{2+} ions are outermost electrons, thus, the emission spectrum of Mn^{2+} ($3d^5$) consists of a broad band varying from green to red color. It is well known that Tanabe-Sugano diagrams are used in coordination chemistry to interpret the characteristics of UV-Vis spectra due to the intra-3*d* shell transition of transition metal ions in host lattice.[47–49] According to the Tanabe-Sugano diagram for the $3d^5$ electron configuration of Mn^{2+}, the energies of the ^4E (^4G), $^4A_1$ (^4G) and ^4E (^4D) excited state relative to the $^6A_1$ (^6S) ground state are insensitive to the crystal-field strength *Dq*, and is determined only by the Racah parameter *B*. The Racah *B* depends greatly on the covalent interaction between Mn^{2+} ions and surrounding ligand and decreases from the free-ion value with increase of the covalent interaction (the nephelauxetic effect[50]). On the other side, the Mn^{2+} ion exhibits a ^6S ground state and the first excited state is a ^4G state, the Tanabe-Sugano diagrams predict that the energy differences between the $^4T_1$ (^4G) and $^4T_2$ (^4G) excited states and the $^6A_1$ (^6S) ground state of Mn^{2+} ions are extremely sensitive to the crystal-field strength *Dq* and decreases with increase of crystal field strength *Dq*. The emission wavelength of Mn^{2+} strongly depends on the crystal field strength of the host lattice. Mn^{2+} usually gives a green emission when it is located on a lattice site with weak crystal field, whereas it exhibits an orange to deep red emission on a strong crystal field site.[26]

Figure 6 shows the excitation and emission spectra of $Ca_{1-x}Mn_xAlSiN_3$ ($x = 0.05$). Under 451 nm excitation, $Ca_{1-x}Mn_xAlSiN_3$ ($x = 0.05$) shows a broad emission band in the wavelength range of 500–800 nm. The observed band emission is ascribed to the $^4T_1$ (^4G) → $^6A_1$ (^6S) transition of Mn^{2+} incorporated

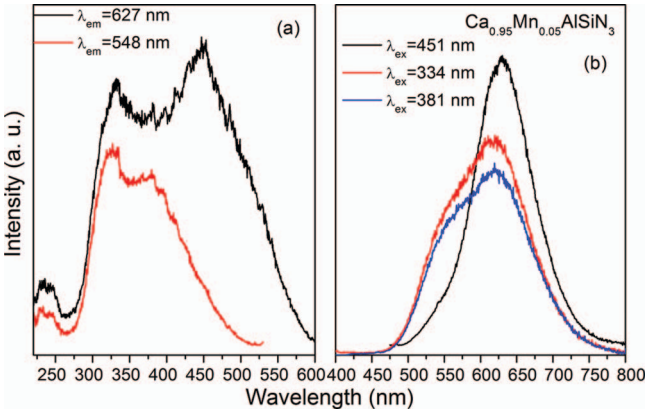

Figure 6. Excitation and emission spectra of $Ca_{1-x}Mn_xAlSiN_3$ ($x = 0.05$).

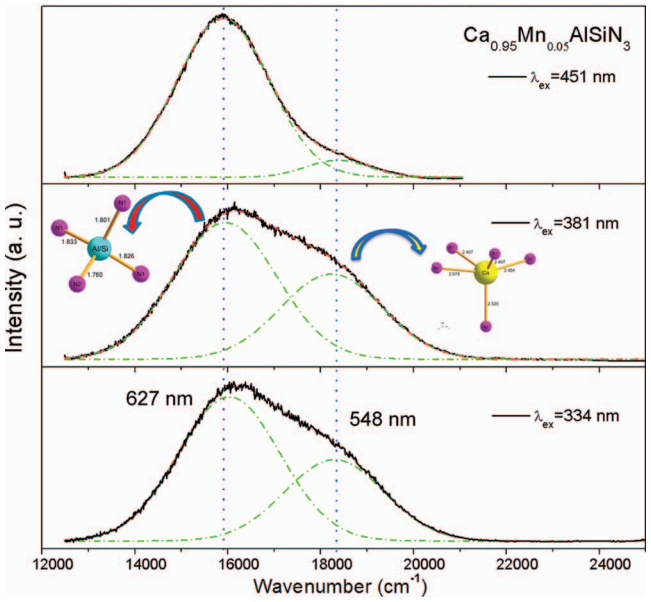

Figure 7. Luminescence spectra of $Ca_{1-x}Mn_xAlSiN_3$ ($x = 0.05$) with deconvoluted Gaussian subbands for emission spectra.

in the $CaAlSiN_3$ host lattice. $^6A_1$ (^6S) is the ground level, and $^4T_1$ (^4G) is the lowest excitation level the energy of which decreases with the increase of the crystal field. Moreover, two obvious overlapping emission sub-bands in the wavelength range of 450–800 nm could be distinguished in the emission spectra of $Ca_{1-x}Mn_xAlSiN_3$ ($x = 0.05$) under 334, 381 and 451 nm excitation (Figure 7). In the crystal structure of $CaAlSiN_3$, there is only one crystallographic site for the Ca atom, which is coordinated with five N atoms (Figure 1). For Eu^{2+} and Ce^{3+}-doped $CaAlSiN_3$, only the Ca sites with strong crystal field strength are substituted by Eu^{2+} and Ce^{3+} ions. As a consequence, a red emission band from Eu^{2+} and yellow-orange emission band from Ce^{3+} are observed in $CaAlSiN_3$.[9,10] Thus, if only the Ca^{2+} sites are substituted by Mn^{2+} ions, it is expected that there will be only a single narrow symmetrical emission band in the luminescence spectra of Mn^{2+}-doped $CaAlSiN_3$. As already mentioned above, however, the emission band is nonsymmetrical, and can be further deconvoluted into two Gaussian subbands with peaks at about 548 nm (18,250 cm^{-1}, green emission) and about 627 nm (15,950 cm^{-1}, red emission), respectively (Figure 7). This indicates that there are two different Mn^{2+} sites in $CaAlSiN_3$ which are ascribed to Mn_{Ca} and Mn_{Al}: not only the Ca^{2+} sites (Mn_{Ca}), but also Al^{3+} sites (Mn_{Al}) can be substituted by Mn^{2+}, which occurs in some other cases.[51,52] Thus, Mn^{2+} ions will be located in a tetrahedrally and pentahedrally nitrogen coordinated site. According to the crystal structure of $CaAlSiN_3$, Al^{3+} site is coordinated with four N atoms with the average Al - N distance 1.8050 Å, which is much smaller than that of Ca^{2+}, coordinated with five N atoms with the average Ca-N distance 2.4934 Å. As a consequence, the crystal field strength is larger for Mn^{2+} at the Al^{3+} site than at the Ca^{2+} site. Considering the Tanabe-Sugano diagram, the emission band at lower energy (15,950 cm^{-1} or 627 nm) is assigned to the Mn^{2+} locating at the Al site (Mn_{Al}), and the other emission band at higher energy (18,250 cm^{-1} or 548 nm) originates from the Mn^{2+} locating at the Ca site (Mn_{Ca}).

There are four principle excitation bands extending over a broad range of wavelengths by monitoring the emission wavelengths of 548 and 627 nm, as shown in Figure 6, which is consistent with the diffuse reflectance spectra. Definitely, the weak excitation band below 275 nm originates from host lattice excitation, which is in agreement with the results published.[39,53] However, it rules out the possibility that there exists efficient energy transfer from $CaAlSiN_3$ host lattice to Mn^{2+} ions due to the weak excitation band from host lattice. There is big difference in the excitation spectra by monitoring the different emission wavelengths : two excitation maxima at 334/451 nm (in the wavelength range of 275–600 nm) and 334/381 nm (in the wavelength range of 275–500 nm) can be observed by monitoring the peak wavelength at 627 and 548 nm, related to Mn^{2+} incorporated on the Al^{3+} site and Ca^{2+} site, respectively. The excitation band of Mn^{2+} consists of several overlapping transitions due to the disordered Al/Si occupation of the same crystallographic position in the $CaAlSiN_3$ lattice. These excitation subbands can be assigned to the transitions of Mn^{2+} at different sites (Mn_{Ca}, Mn_{Al}) from ground state $^6A_1$ (^6S) to $^4T_1$ (^4G), $^4T_2$ (^4G), [$^4A_1$ (^4G), ^4E (^4G)], $^4T_2$ (^4D) and ^4E (^4D) excited states, respectively. Table 1 summarizes the characteristics of $CaAlSiN_3$: Mn^{2+} (5%) phosphor and compares them with other typical Mn^{2+}-doped nitride based phosphors.

Figure 8 shows excitation spectra of $CaAlSiN_3$: Mn^{2+} with different Mn^{2+} doping concentrations. The position of the overall excitation bands in the spectra is nearly independent of the Mn^{2+} concentration, which is similar to that of Eu^{2+} and Ce^{3+} in $CaAlSiN_3$.[9,10] However, the Mn^{2+} concentration exhibits a great effect on the luminescence intensities, as well as the profiles of the emission bands. With increasing Mn^{2+} concentration, the peak positions of the emission bands for

Table I. Characteristics of Mn^{2+}-doped $CaAlSiN_3$ phosphor as compared to typical Mn^{2+}-doped nitride based phosphors at room temperature.

Phosphors	$CaAlSiN_3:Mn^{2+}$	$ZnSiN_2:Mn^{2+}$	$ZnGeN_2:Mn^{2+}$	$MgSiN_2:Mn^{2+}$	$Ca_2Si_5N_8:Mn^{2+}$	$Sr_2Si_5N_8:Mn^{2+}$	$Ba_2Si_5N_8:Mn^{2+}$
Crystal system	*Cmc*2$_1$	*Pna*2$_1$	*Pna*2$_1$	*Pna*2$_1$	*Cc*	*Pmm*2$_1$	*Pmm*2$_1$
Body color	Light red	Gray-white	Gray-white	Gray-white	Gray-white	Gray-white	Gray-white
Host absorption edge (nm)	240	250	376	287	250	265	270
Excitation bands (nm)	275, 334, 381, 451	260, 390, 420, 470, 490	327, 425	360, 380, 430, 465	250, 307, 396, 426, 489	250, 263, 316, 405, 427, 488	248, 261, 290, 436, 405, 421, 486
Emission bands (nm)	548, 627	620	610	625, 692	599	606	567
FWHM (nm)	100	–	130	70	70	60	60
Ref.	This work	32	36	35	34	34	34

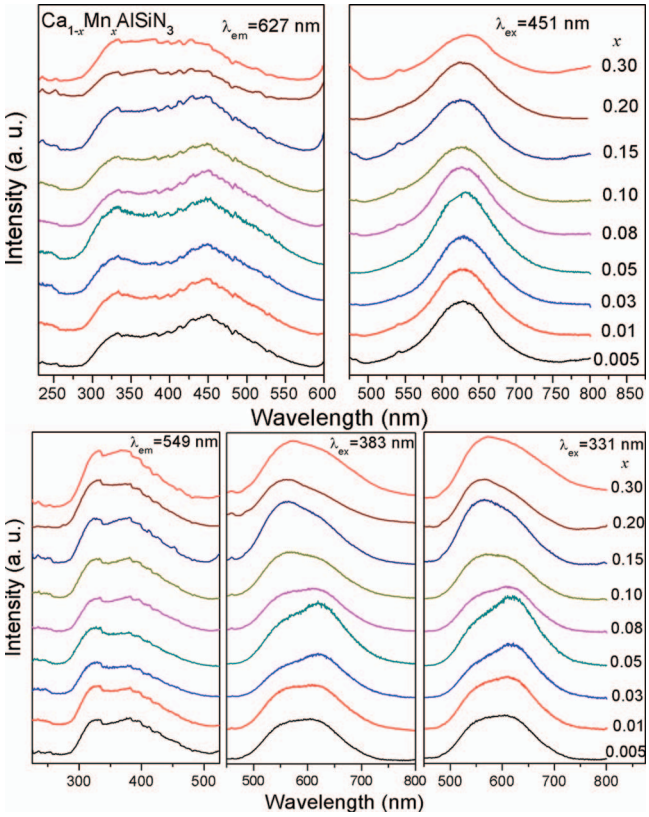

Figure 8. Excitation and emission spectra of $Ca_{1-x}Mn_xAlSiN_3$ ($0.005 \leq x \leq 0.3$) samples.

Mn_{Ca}^{2+} and Mn_{Al}^{2+} sites show a redshift according to the results of fitting the overall emission bands. The redshift of the emission bands of the individual Mn^{2+} centers (Mn_{Ca}, Mn_{Al}) is ascribed to the shrinkage of the host lattice with increasing Mn^{2+} concentration resulting in a larger crystal field strength, and consequently a lower emission energy according to the Tanabe-Sugano diagram. The position of the overall emission band shows a slight redshift (less than 7 nm) under 451 nm excitation. However, a redshift of the overall emission bands under 331/383 nm is observed at low Mn^{2+} concentration ($x < 0.05$), then the overall emission bands exhibit a blueshift with increasing Mn^{2+} concentration ($x > 0.05$). The combination of the redshift of the individual Mn^{2+} centers (Mn_{Ca}, Mn_{Al}) discussed before with the energy transfer from high-energy Mn_{Ca}^{2+} to low-energy Mn_{Al}^{2+} is anticipated to eventually results in the redshift of the overall emission band. The observed blueshift of the overall emission band cannot be explained with the above mentioned effects and therefore is attributed to preferential site occupation of the Ca^{2+} sites with Mn^{2+} for higher Mn-concentrations ($x > 0.05$), resulting in a higher intensity of the high energy Mn^{2+} emission center. Figure 9 shows the overall emission intensity of $CaAlSiN_3 : Mn^{2+}$ as a function of Mn^{2+} concentration under the excitation wavelength of 451 nm and 332 nm. The maximum emission intensity is observed for 5 at% Mn^{2+} doped $CaAlSiN_3$. The overall emission intensity declines gradually as the concentration of Mn^{2+} exceeds 5 at% due to concentration quenching, which is mainly caused by the non-radiative energy transfer among Mn^{2+} ions, which usually occurs as a result of exchange interaction or a multipole - multipole interaction.

The change of the ratio between the emission intensity of the luminescence from Mn_{Al}^{2+} (lower energy, 15,950 cm^{-1} or 627 nm) and Mn_{Ca}^{2+} (higher energy, 18,250 cm^{-1} or 548 nm) is shown in the inset of Figure 9. When Mn^{2+} ions were incorporated into $CaAlSiN_3$, at low concentration ($0 < x \leq 0.05$), not only the Ca^{2+} site, but also the Al^{3+} site can be substituted by Mn^{2+}. As a consequence, emission at lower energy from Mn_{Al}^{2+}, as well as emission at higher energy from Mn_{Ca}^{2+} can be observed, besides, there exists energy transfer from Mn_{Ca}^{2+} to Mn_{Al}^{2+} according to the excitation spectra. Thus, the ratio between the emission intensity of Mn_{Al}^{2+} and Mn_{Ca}^{2+} increases from 0.5 at% Mn^{2+} to 5 at% Mn^{2+}. As the concentration of Mn^{2+} exceeds 5 at% till 15 at%, the ratio declines intensively due to the related concentration quenching of Mn_{Al}^{2+}, then it increases slightly with concentration of Mn^{2+} increasing from 15 at% to 30 at%, which can be ascribed to the related concentration quenching of Mn_{Ca}^{2+} and less concentration quenching for Mn_{Al}^{2+} because most of Mn^{2+} ions will substitute Ca^{2+} ions instead of Al^{3+} at high Mn^{2+} concentration (>15 at%). This is in good agreement with a linear decrease of the unit cell volume with varying Mn^{2+} content (>15 at%).

Figure 10 shows the relative emission intensity of $CaAlSiN_3 : Mn^{2+}$ (5 at%) as a function of sample temperature, using commercial YAG : Ce^{3+} phosphor as a standard for comparison. The quenching temperature T_q (the temperature at which the relative emission

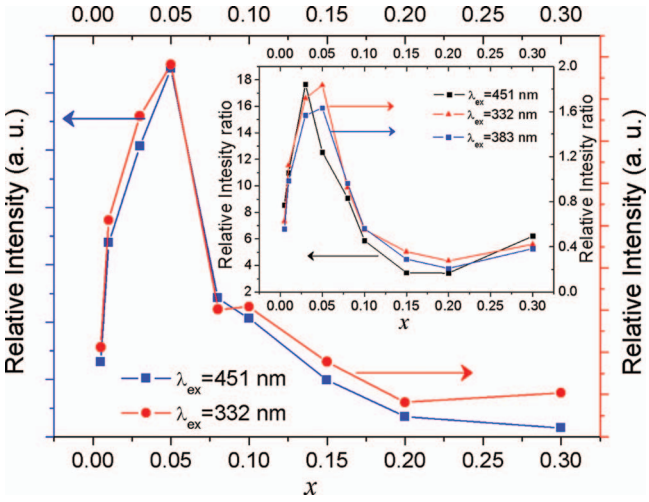

Figure 9. Relative emission intensity of $Ca_{1-x}Mn_xAlSiN_3$ ($0.005 \leq x \leq 0.3$) samples as a function of the Mn^{2+} doping concentration under the excitation wavelength of 451 and 332 nm. The inset shows the change of the ratio between the luminescence intensities of these two emission bands (627 vs. 548 nm) under the excitation wavelength of 451, 383 and 332 nm with increasing Mn^{2+} concentration.

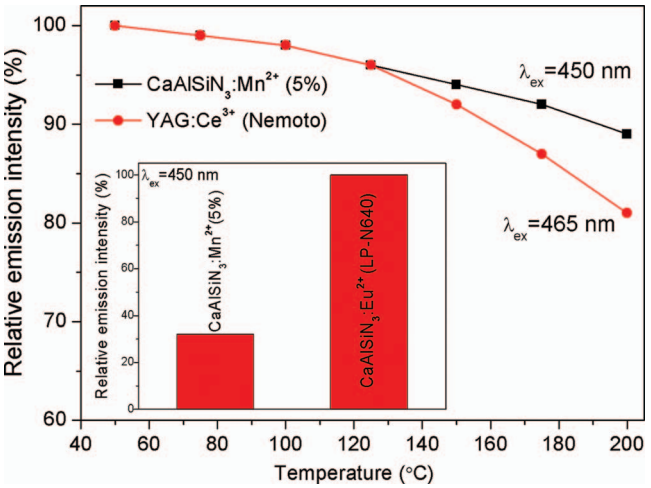

Figure 10. Temperature dependence of the relative emission intensity of $Ca_{1-x}Mn_xAlSiN_3$ ($x = 0.05$) and commercial YAG : Ce^{3+}. The inset shows the relative emission intensity of $CaAlSiN_3 : Mn^{2+}$ (5 at%) compared to the commercial red-emitting phosphor $CaAlSiN_3 : Eu^{2+}$ (LP-N640) under the same conditions.

intensity is half to the initial intensity at room temperature) for $CaAlSiN_3$: Mn^{2+} (5 at%) is above 200°C, which is much better than that of commercial YAG : Ce^{3+} phosphor. In addition, the emission intensity of $CaAlSiN_3$: Mn^{2+} (5 at%) can reach up to about 30% to that of the commercial red-emitting phosphor $CaAlSiN_3$: Eu^{2+} (LP-N640) for excitation with blue light (450 nm) at room temperature, as shown in the inset of Figure 10.

Conclusions

Mn^{2+}-activated $CaAlSiN_3$ phosphors have been prepared by a solid-state reaction successfully and the solubility of Mn^{2+} in host lattice as well as their photoluminescence properties were investigated. $CaAlSiN_3$: Mn^{2+} exhibits a broad band emission in the wavelength range of 475–750 nm. There are two obvious overlapping Mn^{2+} emission bands with peak centers at 548 and 627 nm, which are attributed to the Mn^{2+} locating at the Ca site (Mn_{Ca}) and Al site (Mn_{Al}), respectively. The effect of the Mn^{2+} concentration in $CaAlSiN_3$ on the luminescence properties was investigated and explained on the basis of the presence of the two Mn^{2+} sites, combined with preferential site occupation and energy transfer depending on the Mn^{2+} concentration. $CaAlSiN_3$: Mn^{2+} materials are attractive LED phosphors due to the absorption in the blue range of the spectrum (440–460 nm), efficient luminescence with emission bands in the red part of the spectrum (590–670 nm) and a high thermal quenching temperature in air.

Acknowledgment

The authors gratefully acknowledge financial support from the European Union, the Freistaat Thueringen, the Leuchtstoffwerk Breitungen GmbH (Germany) under contract 2008FE0070 and the National Natural Science Foundation of China under grant No. 11104298. And we thank Dr. Sven Rösler for the temperature dependent luminescence measurement. The authors also gratefully acknowledge Prof. Dr. Yuying Huang and Dr. Xing Gao (SSRF, China) for helpful technical assistance of XANES experiments.

References

1. C. J. Duan, X. J. Wang, W. M. Otten, A. C. A. Delsing, J. T. Zhao, and H. T. Hintzen, *Chemistry of Materials*, **20**, 1597 (2008).
2. V. Bachmann, T. Jüstel, A. Meijerink, C. Ronda, and P. J. Schmidt, *Journal of Luminescence*, **121**, 441 (2006).
3. Y. Q. Li, J. E. J. van Steen, J. W. H. van Krevel, G. Botty, A. C. A. Delsing, F. J. DiSalvo, G. de With, and H. T. Hintzen, *Journal of Alloys and Compounds*, **417**, 273 (2006).
4. R. J. Xie, N. Hirosaki, T. Suehiro, F. F. Xu, and M. Mitomo, *Chemistry of Materials*, **18**, 5578 (2006).
5. Y. Q. Li, G. de With, and H. T. Hintzen, *Journal of Solid State Chemistry*, **181**, 515 (2008).
6. Y. Q. Li, G. de With, and H. T. Hintzen, *Journal of Luminescence*, **116**, 107 (2006).
7. M. Zeuner, P. J. Schmidt, and W. Schnick, *Chemistry of Materials*, **21**, 2467 (2009).
8. K. S. Sohn, S. Lee, R. J. Xie, and N. Hirosaki, *Applied Physics Letters*, **95**, 121903 (2009).
9. K. Uheda, N. Hirosaki, Y. Yamamoto, A. Naito, T. Nakajima, and H. Yamamoto, *Electrochemical Solid Solid-State Letters*, **9**, H22 (2006).
10. Y. Q. Li, N. Hirosaki, R. J. Xie, T. Takeda, and M. Mitomo, *Chemistry of Materials*, **20**, 6704 (2008).
11. H. Watanabe, H. Wada, K. Seki, M. Itou, and N. Kijima, *Journal of the Electrochemical Society*, **155**, F31 (2008).
12. H. Watanabe and N. Kijima, *Journal of Alloys and Compounds*, **475**, 434 (2009).
13. R. J. Xie, M. Mitomo, K. Uheda, F. F. Xu, and Y. Akimune, *Journal of the American Ceramic Society*, **85**, 1229 (2002).
14. R. J. Xie, N. Hirosaki, K. Sakuma, Y. Yamamoto, and M. Mitomo, *Applied Physics Letters*, **84**, 5404 (2004).
15. R. J. Xie, N. Hirosaki, M. Mitomo, Y. Yamamoto, T. Suehiro, and K. Sakuma, *Journal of Physical Chemistry B*, **108**, 12027 (2004).
16. R. J. Xie, N. Hirosaki, M. Mitomo, K. Takahashi, and K. Sakuma, *Applied Physics Letters*, **88**, 101104 (2006).
17. Y. Q. Li, A. C. A. Delsing, G. de With, and H. T. Hintzen, *Chemistry of Materials*, **17**, 3242 (2005).
18. Y. Q. Li, G. de With, and H. T. Hintzen, *Journal of Materials Chemistry*, **15**, 4492 (2005).
19. Y. Q. Li, G. de With, and H. T. Hintzen, *Journal of the Electrochemical Society*, **153**, G278 (2006).
20. Y. Q. Li, N. Hirosaki, R. J. Xie, T. Takeda, and M. Mitomo, *Journal of Solid State Chemistry*, **181**, 3200 (2008).
21. J. W. H. van Krevel, H. T. Hintzen, R. Metselaar, and A. Meijerink, *Journal of Alloys and Compounds*, **268**, 272 (1998).
22. R. J. Xie, N. Hirosaki, and M. Mitomo, *Journal of Electroceramics*, **21**, 370 (2008).
23. Y. F. Lin, Y. H. Chang, Y. S. Chang, B. S. Tsai, and Y. C. Li, *Journal of Alloys and Compounds*, **421**, 268 (2006).
24. A. L. Smith, *Journal of the Electrochemical Society*, **98**, 363 (1951).
25. J. K. Berkowitz and J. A. Olsen, *Journal of Luminescence*, **50**, 111 (1991).
26. G. Blasse and B. C. Grabmaier, *Luminescent Materials*: Springer-Verlag, Berlin, 1994.
27. X. M. Zhang, H. P. Zeng, and Q. Su, *Journal of Alloys and Compounds*, **441**, 259 (2007).
28. D. Y. Lee, Y. C. Kang, H. D. Park, and S. K. Ryu, *Journal of Alloys and Compounds*, **353**, 252 (2003).
29. R. P. Sreekanth Chakradhar, B. M. Nagabhushana, K. P. Ramesh, and J. L. Rao, *Journal of Chemical Physics*, **121**, 10250 (2004).
30. Y. Hattori, T. Isobe, H. Takahashi, and S. Itoh, *Journal of Luminescence*, **113**(1-2), 69 (2005).
31. Y. Takahashi and T. Isobe, *Japanese Journal of Applied Physics Part 1*, **442**(2), 922 (2005).
32. K. Uheda, H. Takizawa, and T. Endo, *Journal of Materials Science Letters*, **20**, 1753 (2001).
33. V. Bonder, L. Axelrud, V. Davydov, and T. Felter, *Materials Research Society Symposium Proceedings*, **639**, G11.36.1 (2001).
34. C. J. Duan, W. M. Otten, A. C. A. Delsing, and H. T. Hintzen, *Journal of Solid State Chemistry*, **181**, 751 (2008).
35. C. J. Duan, A. C. A. Delsing, and H. T. Hintzen, *Journal of Luminescence*, **129**, 645 (2009).
36. Q. H. Zhang, J. Wang, C. W. Yeh, W. C. Ke, R. S. Liu, J. K. Tang, M. B. Xie, H. B. Liang, and Q. Su, *Acta Materialia*, **58**, 6728 (2010).
37. R. J. Xie, N. Hirosaki, X. J. Liu, T. Takeda, and H. L. Li, *Applied Physics Letters*, **92**, 201905 (2008).
38. C. Kulshreshtha, J. H. Kwak, Y. J. Park, and K. S. Sohn, *Optical Letters*, **34**, 794 (2009).
39. K. Uheda, N. Hirosaki, and H. Yamamoto, *Physica Status Solidi (a)*, **203**, 2712 (2006).
40. X. Q. Piao, K. I. Machida, T. Horikawa, H. Hanzawa, Y. Shimomura, and N. Kijima, *Chemistry of Materials*, **19**, 4592 (2008).
41. N. Hirosaki, K. Sakuma, K. Ueda, and H. Yamamoto, WO 2005/078811.
42. J. Rodriguez-Carvajal, *Fullprof*, Institute Laue-Langervin: Grenoble, France. July, 2006.
43. R. D. Shannon, *Acta Crystallographica*, **751**, A32 (1976).
44. D. P. Thompson, *Materials Science Forum*, **47**, 21 (1989).
45. M. Mikami, K. Uheda, and N. Kijima, *Physica Status Solidi*, **203**, 2705 (2006).
46. Y. R. Lee, A. K. Ramdas, and R. L. Aggarwal, *Physical Review B*, **38**, 10600 (1988).
47. Y. Tanabe and S. Sugano, *Journal of the Physical Society of Japan*, **9**, 753 (1954).
48. Y. Tanabe and S. Sugano, *Journal of the Physical Society of Japan*, **9**, 766 (1954).
49. Y. Tanabe and S. Sugano, *Journal of the Physical Society of Japan*, **11**, 864 (1956).
50. J. S. Griffith, *The Theory of Transition-Metal Ions*, Cambridge University Press, Cambridge, 1961.
51. A. Bergstein and W. B. White, *Journal of the Electrochemical Society*, **118**, 1166 (1971).
52. Y. H. Won, H. S. Jang, W. B. Im, D. Y. Jeon, and J. S. Lee, *Applied Physics Letters*, **89**, 231909 (2006).
53. Z. J. Zhang, O. M. t. Kate, A. C. A. Delsing, E. v. d. Kolk, P. H. L. Notten, P. Dorenbos, J. T. Zhao, and H. T. Hintzen, *Journal of Materials Chemistry*, **22**, 9813 (2012).